Applied Mathematics and Computation 341 (2019) 288–300

Contents lists available at ScienceDirect

Applied Mathematics and Computation

journal homepage: www.elsevier.com/locate/amc

Analysis of the stability and dispersion for a Riemannian acoustic wave equation

H.R. Quiceno[a,*], C. Arias[b]

[a] C3, Instituto Tecnológico Metropolitano ITM, Universidad EAFIT, Colombia
[b] C3, Instituto Tecnológico Metropolitano ITM, Universidad de Antioquia, Colombia

ARTICLE INFO

Keywords:
Finite difference scheme
Courant–Friedrich–Lewy stability condition
Von-Neumann stability criteria
Riemannian acoustic wave equation

ABSTRACT

The construction of images of the Earth's interior using methods as reverse time migration (RTM) or full wave inversion (FWI) strongly depends on the numerical solution of the wave equation. A mathematical expression of the numerical stability and dispersion for a particular wave equation used must be known in order to avoid unbounded numbers of amplitudes. In case of the acoustic wave equation, the Courant–Friedrich–Lewy (CFL) condition is a necessary but is not a sufficient condition for convergence. Thus, we need to search other types of expression for stability condition. In seismic wave problems, the generalized *Riemannian wave equation* is used to model their propagation in domains with curved meshes which is suitable for zones with rugged topography. However, only a heuristic version of stability condition was reported in the literature for this equation. We derived an expression for stability condition and numerical dispersion analysis for the Riemannian acoustic wave equation in a two-dimensional medium and analyzed its implications in terms of computational cost.

1. Introduction

One of the most important features when simulating wave propagation into the earth is to design stable, accurate and efficient numerical methods which represent the propagation phenomena and generate images of the earths interior which represent its constitution, geometry, and layers distribution. Some of the methods that recently have been used to simulate acoustic wave propagation in different scenarios and with several boundary conditions are [8] where the boundary element method is used to solve 3D acoustic scattering; [13] used a hybrid methodology combining the finite element method and the wave based method to maximize the advantages and compensate the drawbacks of both numerical methods; [3] developed the singular boundary method for wave propagation analysis to eliminate singularities of the fundamental solutions and numerical evaluation of the singular integrals in the boundary element method. Nevertheless, the most straightforward method is the finite-difference time-domain (FDTD) approximation of the solution of the wave equation simulated on rectangular meshes. This method faces some difficulties to properly model the earth since the geological structures of the earth are described by rectangular meshes but the data acquisition can be made on irregular surfaces or rugged topography and this important aspect is not considered usually into the FDTD method.

* Corresponding author.
E-mail address: romanquiceno@gmail.com (H.R. Quiceno).

https://doi.org/10.1016/j.amc.2018.08.047
0096-3003/

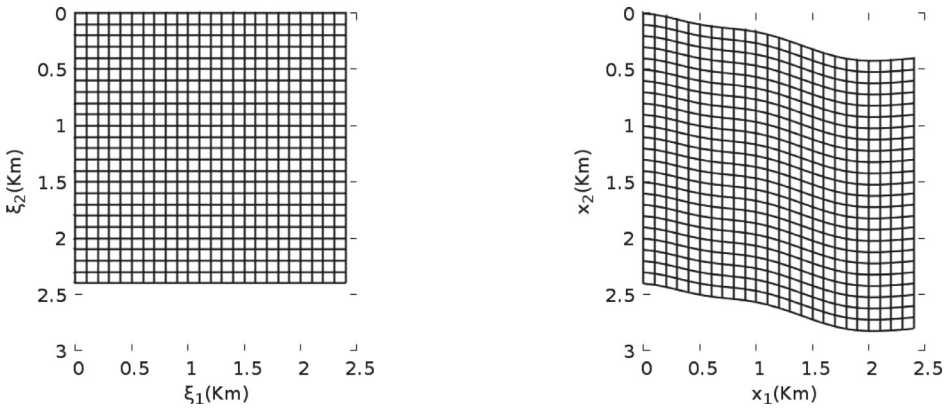

(a) Computational domain (b) Physical domain

Fig. 1. The transformation of coordinates given by equations $\boldsymbol{\phi}$ allows to go from (a) to (b).

One way to include the topography of the acquisition surface is to perform a conformal transformation from a domain with a curved upper surface to a rectangular Cartesian grid. The strategy of conformally transform the grids has been developed by many authors in curvilinear coordinates, for instance see [1,7,17], for the elastic wave equation and [18] for the acoustic wave equation. In these works the wave equation is transformed (a smooth coordinate transformation) to be implemented in a cartesian grid which conforms with a curved irregular grid, an orthogonality condition is possed and then some terms with mixed partial derivatives of the wavefield vanish, and the result is a wave equation with a transformed Laplacian operator. A FDTD scheme is used, and a stability condition is derived by Fourier analysis of the components of the wavefield. [1], established a second order stable finite difference scheme for the elastic wave equation in a curvilinear system, showing that the spatial operators in the method are self-adjoint for free-surface, nevertheless, the authors do not present a stability criteria. Recently in [20], the Von-Neumann method was applied for stability and numerical dispersion for a FD scheme for the diffusive-viscous wave equation, in that work the results obtained were compared with stability condition for the acoustic case and revealed that the stability condition is more restrictive for the diffusive-viscous case on which a smaller time step is required but numerical dispersion is also smaller than that in the acoustic case.

Nevertheless this approaches are dependent of the Euclidean structure to describe distances, angles between rays, overturning rays, the symmetries that the continuum may posses, among other issues. To properly describe the continuum in terms of its material symmetries and the tensor operators that are naturally defined on it, it is necessary to provide a general geometrical structure on which the propagation can be described in a general way. Riemannian geometry is one of the general structures which allows us to formally describe an elastic boby and to obtain the equations of motion after a deformation, see [9,12] proposed a Riemannian wave equation, as a pure eigenvalue equation by considering the Laplace–Beltrami operator acting on a pressure field. [16] included the topography geometry in the acoustic Riemannian wave equation and, [15] developed a FD scheme with conformal transformations of the domains. In this work, a stability condition is derived in a heuristic way taking as the starting point the CFL stability condition and transforming it by means of the chain rule. Formally, this is not a stability condition since it is not including the area and distances transformations, which are geometrical aspects intrinsically included in the metric tensor defined in a Riemannian manifold, and the time sampling resulting from this analysis to ensure stability of the FDTD scheme is quite far of being optimal.

Our aim is to apply the Von-Neumann method to obtain a stability criteria for a second order and fourth order FD scheme of the 2D Riemannian acoustic wave equation and compare it with the heuristic one used by Shragge (2014). For numerical comparison, we also perform a wave propagation using two different topography profiles: a Gaussian 2D profile and the Canadian Foothills profile, ([5]), a synthetic velocity model representing a zone in the British Columbia (Canada) that shows several geological complexities common in that region. This velocity model allows us to show the dependence of the stability criteria on the smoothness of the profile. Finally we analyze the numerical dispersion for the generalized wave equation and compare it with the Cartesian acoustic wave equation.

2. 2D Riemannian wave equation

In this section we make a review of the formulation of the Riemannian wave equation which agrees with the wave equations used by [12,14,15]. For a basic study on Riemannian manifolds the reader is referred to [10] and for the elastic formulation on Riemannian manifolds see [9].

Let $\boldsymbol{x} = [x_1, x_2]^T$ be coordinates of a curved physical domain on which we want to solve the wave equation (Fig. 1b) and, $\boldsymbol{\xi} = [\xi_1, \xi_2]^T$ a rectangular (regular) computational domain on which we actually compute the acoustic wavefield (Fig. 1a). Consider a function $\boldsymbol{x} = \boldsymbol{\phi}(\boldsymbol{\xi})$ that maps the computational domain onto the physical domain and the constant-density

acoustic wave equation in a 2D Riemannian coordinate system defined by

$$\nabla^2_{\boldsymbol{\xi}} U_{\boldsymbol{\xi}} - \frac{1}{v^2_{\boldsymbol{\xi}}} \frac{\partial^2 U_{\boldsymbol{\xi}}}{\partial t^2} = F_{\boldsymbol{\xi}}, \tag{1}$$

where $U_{\boldsymbol{\xi}} = U(\boldsymbol{\phi}(\boldsymbol{\xi}), t)$ is a scalar wave field, the scalar $v_{\boldsymbol{\xi}} = v(\boldsymbol{\phi}(\boldsymbol{\xi}))$ is the wave velocity and $F_{\boldsymbol{\xi}} = F(\boldsymbol{\phi}(\boldsymbol{\xi}), t)$ is the source distribution. The Jacobian of $\boldsymbol{\phi}$ is

$$\mathbf{J} = \frac{\partial \boldsymbol{\phi}}{\partial \boldsymbol{\xi}}, \tag{2}$$

and the Laplace–Beltrami operator $\nabla^2_{\boldsymbol{\xi}}$ is described as [6]

$$\nabla^2_{\boldsymbol{\xi}} = \sum_{j=1}^{2} \sum_{l=1}^{2} \frac{1}{\sqrt{|\mathbf{g}|}} \frac{\partial}{\partial \xi_j} \left(g^{jl} \sqrt{|\mathbf{g}|} \frac{\partial}{\partial \xi_l} \right), \tag{3}$$

where $|\mathbf{g}| = \det[g_{jl}]$ is the determinant of g_{jl} with

$$[g_{jl}] = \mathbf{J}^T \mathbf{J} \quad \text{and} \quad [g^{jl}] = \left[g_{jl} \right]^{-1}. \tag{4}$$

Let us take the coordinate transformation mapping $\boldsymbol{\phi}$ as a diffeomorphism (it is an invertible and smooth function whose inverse is smooth too) the basic question on that manifold is if the Jacobian $\mathbf{J}$ preserves area (volume), that is,

$$\det[\mathbf{J}] = 1, \quad \text{that implies} \quad |\mathbf{g}| = 1. \tag{5}$$

Eq. (5) makes the Laplace–Beltrami operator a good candidate to formulate acoustic wave equations on a Riemannian manifold. Note that the transformation $\boldsymbol{\phi}$ is a mapping that transforms the computational domain onto the physical domain in a bijective way, preserving the area, and is at least twice differentiable. Using that transformation, we find a new expression for the Laplace–Beltrami operator on the computational domain $\boldsymbol{\xi}$ to propose an acoustic wave equation.

Expanding the Laplace–Beltrami operator, we can re-write Eq. (3) in a more convenient way, as

$$\nabla^2_{\boldsymbol{\xi}} = \sum_{j=1}^{2} \sum_{l=1}^{2} \left[g^{jl} \frac{\partial^2}{\partial \xi_j \partial \xi_l} \right] + \zeta^1 \frac{\partial}{\partial \xi_1} + \zeta^2 \frac{\partial}{\partial \xi_2}, \tag{6}$$

and as $\sqrt{|\mathbf{g}|} = 1$, where

$$\zeta^l = \sum_{j=1}^{2} \frac{\partial g^{lj}}{\partial \xi_j}. \tag{7}$$

Therefore, using Eqs. (6) and (7) in Eq. (1), we have the Riemannian acoustic 2D wave equation given by

$$\left[g^{11} \frac{\partial^2 U_{\boldsymbol{\xi}}}{\partial \xi_1^2} + 2 g^{12} \frac{\partial^2 U_{\boldsymbol{\xi}}}{\partial \xi_1 \partial \xi_2} + g^{22} \frac{\partial^2 U_{\boldsymbol{\xi}}}{\partial \xi_2^2} + \zeta^1 \frac{\partial U_{\boldsymbol{\xi}}}{\partial \xi_1} + \zeta^2 \frac{\partial U_{\boldsymbol{\xi}}}{\partial \xi_2} \right] - \frac{1}{v^2_{\boldsymbol{\xi}}} \frac{\partial^2 U_{\boldsymbol{\xi}}}{\partial t^2} = F_{\boldsymbol{\xi}}. \tag{8}$$

Surface topography problem

The use of this coordinate transformation approach, allows to compute the acoustic wave propagation in topographic coordinates.

The transformation that maps the rectangular domain onto the physical domain is given by

$$\begin{cases} x_1 = \phi_1(\xi_1, \xi_2) = \xi_1; \\ x_2 = \phi_2(\xi_1, \xi_2) = \xi_2 + \psi(\xi_1), \end{cases} \tag{9}$$

where ψ is a smooth function that represents the curved upper boundary of the physical domain. This function must be, at least, twice differentiable. Thus, under that condition the function $\boldsymbol{\phi} = (\phi_1, \phi_2)$ is a coordinate chart for the physical domain which is being modeled on a regular Euclidean space (see, Fig. 1). The elements $\zeta^{\mathbf{i}}$ are geometric factors as the $g's$, so they have to be calculated only one time. For the specific transformation given in Eq. (9), we have:

$$[g_{ij}] = \begin{bmatrix} \left(1 + (\psi')^2\right) & \psi' \\ \psi' & 1 \end{bmatrix}, \quad [g^{ij}] = \begin{bmatrix} 1 & -\psi' \\ -\psi' & \left(1 + (\psi')^2\right) \end{bmatrix} \quad \text{and} \quad |\mathbf{g}| = 1. \tag{10}$$

The ζ^j coefficients are explicitly given by

$$\zeta^1 = \frac{\partial g^{11}}{\partial \xi_1} + \frac{\partial g^{12}}{\partial \xi_2} = 0\,,$$
$$\zeta^2 = \frac{\partial g^{21}}{\partial \xi_1} + \frac{\partial g^{22}}{\partial \xi_2} = -\psi''\,. \tag{11}$$

Therefore, using Eqs. (10) and (11) in Eq. (8), we get

$$\left[\frac{\partial^2 U_\xi}{\partial \xi_1^2} - 2\psi'\frac{\partial^2 U_\xi}{\partial \xi_1 \partial \xi_2} + \left[1+(\psi')^2\right]\frac{\partial^2 U_\xi}{\partial \xi_2^2} - \psi''\frac{\partial U_\xi}{\partial \xi_2}\right] - \frac{1}{v_\xi^2}\frac{\partial^2 U_\xi}{\partial t^2} = F_\xi\,, \tag{12}$$

noting that ψ' and ψ'' are functions of ξ_1.

3. 2D-second order Riemannian wave equation FD scheme

The finite-difference method is the most straightforward numerical approach used in seismic modeling due to its relative accuracy and computational efficiency, nevertheless, the size of the time step is bounded by a stability criterion which is an important factor affecting the accuracy of the results. This bound depends on the grid spacing and particularly, for the Riemannian 2D wave equation, it also depends on geometrical factors.

3.1. Von-Neumann stability criteria of Riemannian 2D wave equation

The stability condition for the acoustic wave equation is widely known as the Courant–Friderichs–Lewy condition (CFL), formely developed in 1928 [2] and can be found in novel works on seismic migration such as [4,11,19], among others. In Cartesian two dimensional spaces this condition is given by

$$\Delta t \le \frac{\Delta r}{v(\mathbf{x})}, \tag{13}$$

where

$$\Delta r = \left[\Delta x_1^{-2} + \Delta x_2^{-2}\right]^{-\frac{1}{2}} \tag{14}$$

is the root-mean-square (RMS) of the spatial sampling and $v(\mathbf{x})$ is the maximum value of the velocity model in the physical grid.

In the Riemannian case, the only approach to it has been made by [15], who uses the chain rule in Eq. (13) to get the expression:

$$\Delta t \le \frac{1}{v_\xi} \times \arg\min_{\xi}\left\{\left[\left(\frac{\partial \phi_1}{\partial \boldsymbol{\xi}^T}\Delta\boldsymbol{\xi}\right)^{-2} + \left(\frac{\partial \phi_2}{\partial \boldsymbol{\xi}^T}\Delta\boldsymbol{\xi}\right)^{-2}\right]^{-\frac{1}{2}}\right\}. \tag{15}$$

To derive the appropriated stability condition we make use of the Von-Neumann method as follows:

The differential operators in Eq. (8), are expanded in a second order finite difference scheme as:

$$\begin{aligned}
\frac{\partial^2 U_\xi}{\partial t^2} &= \frac{U_{\nu,k}^{n+1} - 2U_{\nu,k}^{n} + U_{\nu,k}^{n-1}}{(\Delta t)^2}\,,\\
\frac{\partial^2 U_\xi}{\partial \xi_1 \partial \xi_2} &= \frac{U_{\nu+1,k+1}^{n} - U_{\nu-1,k+1}^{n} - U_{\nu+1,k-1}^{n} + U_{\nu-1,k-1}^{n}}{4\Delta\xi_1\Delta\xi_2}\,,\\
\frac{\partial^2 U_\xi}{\partial \xi_1^2} &= \frac{U_{\nu+1,k}^{n} - 2U_{\nu,k}^{n} + U_{\nu-1,k}^{n}}{(\Delta\xi_1)^2}\,,\\
\frac{\partial^2 U_\xi}{\partial \xi_2^2} &= \frac{U_{\nu,k+1}^{n} - 2U_{\nu,k}^{n} + U_{\nu,k-1}^{n}}{(\Delta\xi_2)^2}\,,\\
\frac{\partial U_\xi}{\partial \xi_1} &= \frac{U_{\nu+1,k}^{n} - U_{\nu-1,k}^{n}}{2\Delta\xi_1}\,,\\
\frac{\partial U_\xi}{\partial \xi_2} &= \frac{U_{\nu,k+1}^{n} - U_{\nu,k-1}^{n}}{2\Delta\xi_2},
\end{aligned} \tag{16}$$

where n, ν, and k are the discretization variables for t, ξ_1, and ξ_2, respectively.

The system of Eq. (16) replaced in the acoustic wave Eq. (1) with $F_\xi = 0$ produces the recursive scheme

$$\begin{aligned} U_{\nu,k}^{n+1} = & -U_{\nu,k}^{n-1} - \frac{\Delta t^2 v_\xi^2}{2\Delta\xi_1^2\Delta\xi_2^2}\big[-\Delta\xi_1\Delta\xi_2 U_{\nu-1,k-1}^{n} g_{12} + \Delta\xi_1\Delta\xi_2 U_{\nu-1,k+1}^{n} g_{12} \\ & + \Delta\xi_1\Delta\xi_2 U_{\nu+1,k-1}^{n} g_{12} - \Delta\xi_1\Delta\xi_2 U_{\nu+1,k+1}^{n} g_{12} \\ & + U_{\nu,k}^{n}(-4\Delta\xi_1^2\Delta\xi_2^2 + 4\Delta\xi_2^2 g_{11} + 4\Delta\xi_2^2 g_{22}) \\ & + (U_{\nu+1,k}^{n} + U_{\nu-1,k}^{n})(-2\Delta\xi_2^2 g_{11} - \Delta\xi_1\Delta\xi_2^2\zeta_1) \\ & + (U_{\nu,k+1}^{n} + U_{\nu,k-1}^{n})(-2\Delta\xi_1^2 g_{22} - \Delta\xi_1^2\Delta\xi_2\zeta_2)\big], \end{aligned} \tag{17}$$

valid up to order two in space and time. Now, consider a trial solution in the form

$$U_{\nu,k}^{n} = u_{\nu,k}^{n} + \epsilon_{\nu,k}^{n}, \tag{18}$$

where U_ξ is the exact solution (if it exists), u is the solution approximation and ϵ is the error introduced up to the desired order when approximating the solution. Assuming that Eq. (17) admits harmonic solutions in the form:

$$u_{\nu,k}^{n} = u^n e^{i(\kappa_1 \nu\Delta\xi_1 + \kappa_2 k\Delta\xi_2)}, \tag{19}$$

where $i = \sqrt{-1}$ is the imaginary number and κ_1, and κ_2 are wave numbers, we can expect that the error behaves in the same way:

$$\epsilon_{\nu,k}^{n} = \epsilon^n e^{i(\kappa_1 \nu\Delta\xi_1 + \kappa_2 k\Delta\xi_2)}. \tag{20}$$

Inserting Eq. (18) in the FD scheme Eq. (17) and taking into account that u satisfies the wave equation within the specified order of accuracy, the resulting equation only involves ϵ:

$$\begin{aligned} \epsilon_{\nu,k}^{n+1} = & 2\epsilon_{\nu,k}^{n} - \epsilon_{\nu,k}^{n-1} + \epsilon_{\nu,k}^{n}(v_\xi\Delta t)^2\left(\frac{\zeta^1}{\Delta\xi_1} i\sin(\kappa_1\Delta\xi_1) + \frac{\zeta^2}{\Delta\xi_2} i\sin(\kappa_2\Delta\xi_2) + \frac{g^{11}}{(\Delta\xi_1)^2}[2\cos(\kappa_1\Delta\xi_1) - 2]\right. \\ & \left. + \frac{g^{22}}{(\Delta\xi_2)^2}[2\cos(\kappa_2\Delta\xi_2) - 2] + \frac{g^{12}}{2\Delta\xi_1\Delta\xi_2} 2i\sin(\kappa_1\Delta\xi_1) 2i\sin(\kappa_2\Delta\xi_2)\right), \end{aligned} \tag{21}$$

that can be written as

$$\epsilon^{n+1} = B\epsilon^n - \epsilon^{n-1}. \tag{22}$$

Denote

$$R = \frac{\epsilon^{n+1}}{\epsilon^n} = \frac{\epsilon^n}{\epsilon^{n-1}}, \tag{23}$$

then the previous expression is written as $R^2 - BR + 1 = 0$, from which

$$R = \frac{B \pm \sqrt{B^2 - 4}}{2}. \tag{24}$$

We want ϵ^n, to be decreasing, so $|R| \le 1$, and this implies that the stability condition for the 2D Riemannian wave equation is

$$\left| B \pm \sqrt{B^2 - 4} \right| \le 2. \tag{25}$$

If B is real, this expression could be replaced by two inequalities that would allow to solve for Δt. Nevertheless we should evaluate this inequality numerically since it is not possible to solve for Δt because it contains nonstationary terms associated with the metric tensor, explicitly depends on the space variables and, contains complex terms arising from mixed derivatives.

For each fixed x_1-value, we calculate B from Eq. (21), for a range of Δt from 0 to a value above the CFL-limit. In this interval we take about a hundred values in an increasing way and, select for each value of x_1 the maximum Δt that satisfies the inequality 25; the results of this procedure are shown in Figs. 4 and 8 for two different topographic profiles.

We also calculate the stability condition for the generalized acoustic wave equation using 4th order finite differences equations for the spatial derivatives. Again we obtain a relation between ϵ^{n+1}, ϵ^n and ϵ^{n-1}, because they come from the second derivative in time which is still approximated in a second order finite-difference equation. Then, this produces a 2^{nd} order polynomial in R, therefore a stability condition similar to (25) given by the expression:

$$\begin{aligned} B = 2 + v^2(\Delta t)^2 \Bigg\{ & \left(\frac{2\cos(\kappa_1\Delta\xi_1)\sin^2\left(\frac{1}{2}\kappa_1\Delta\xi_1\right)}{3\Delta\xi_1^2} - \frac{14\sin^2\left(\frac{1}{2}\kappa_1\Delta\xi_1\right)}{3\Delta\xi_1^2} \right) g_{11} \\ & + \left(\frac{4\sin(2\kappa_1\Delta\xi_1)\sin(\kappa_2\Delta\xi_1)}{9\Delta\xi_1\Delta\xi_2} - \frac{32\sin(\kappa_1\Delta\xi_1)\sin(\kappa_2\Delta\xi_2)}{9\Delta\xi_1\Delta\xi_2} \right. \end{aligned}$$

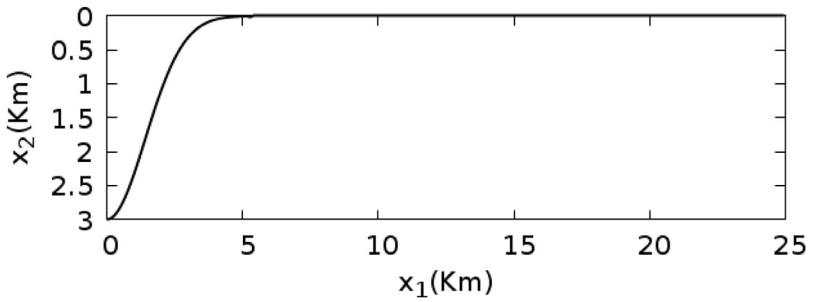

Fig. 2. Mountain profile given by $\psi(x_1) = he^{-a^2x_1^2}$.

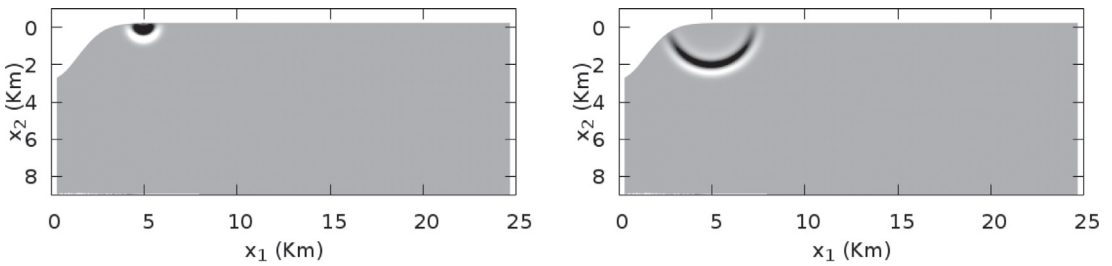

(a) Propagation of the Ricker pulse at 30 ms

(b) Propagation of the Ricker pulse at 60 ms

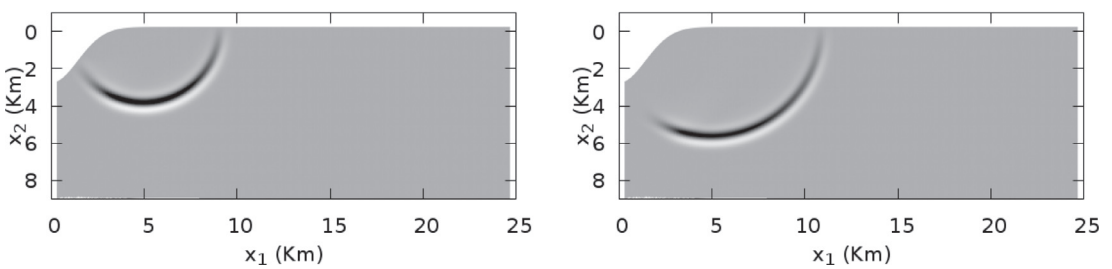

(c) Propagation of the Ricker pulse at 90 ms

(d) Propagation of the Ricker pulse at 120 ms

Fig. 3. Snapshot for the propagation of a Ricker pulse in a medium with constant velocity and a upper boundary given by $\psi(x_1) = he^{-a^2x_1^2}$. The value of Δt used for the propagation is $4 \times 10^{-3}s$, which is in agreement with the numeric limit shown in Fig. 4 but not with the heuristic limit.

$$
\begin{aligned}
&+\frac{\sin(\kappa_1\Delta\xi_1)\sin(2\kappa_2\Delta\xi_2)}{9\Delta\xi_1\Delta\xi_2}-\frac{\sin(2\kappa_1\Delta\xi_1)\sin(2\kappa_2\Delta\xi_2)}{18\Delta\xi_1\Delta\xi_2}\Bigg)g_{12} \\
&+\left(\frac{\cos(\kappa_2\Delta\xi_2)\sin^2\left(\frac{1}{2}\kappa_2\Delta\xi_1\right)}{3\Delta\xi_2^2}-\frac{14\sin^2\left(\frac{1}{2}\kappa_1\Delta\xi_1\right)}{3\Delta\xi_2^2}\right)g_{11} \\
&+i\left(\frac{4\sin(\kappa_1\Delta\xi_1)}{3\Delta\xi_2}-\frac{\sin(2\kappa_1\Delta\xi_1)}{6\Delta\xi_1}\right)+i\left(\frac{4\sin(\kappa_2\Delta\xi_2)}{3\Delta\xi_2}-\frac{\sin(2\kappa_2\Delta\xi_2)}{6\Delta\xi_2}\right)\Bigg\}
\end{aligned}
\tag{26}
$$

3.2. Numerical dispersion analysis

The numerical dispersion analysis is performed by the relation between the phase velocity and the frequency or equivalently, between phase velocity and the number of points per wavelength (ppw). In the absence of dispersion, the phase velocity is constant. To find this relation, the plane wave solution (19) is substituted in Eq. (17) which, up to order 2, gives the following equation:

$$e^n_{\nu,k} = e^{i(\kappa_1\nu\Delta\xi_1+\kappa_2 k\Delta\xi_2-\omega n\Delta t)}. \tag{27}$$

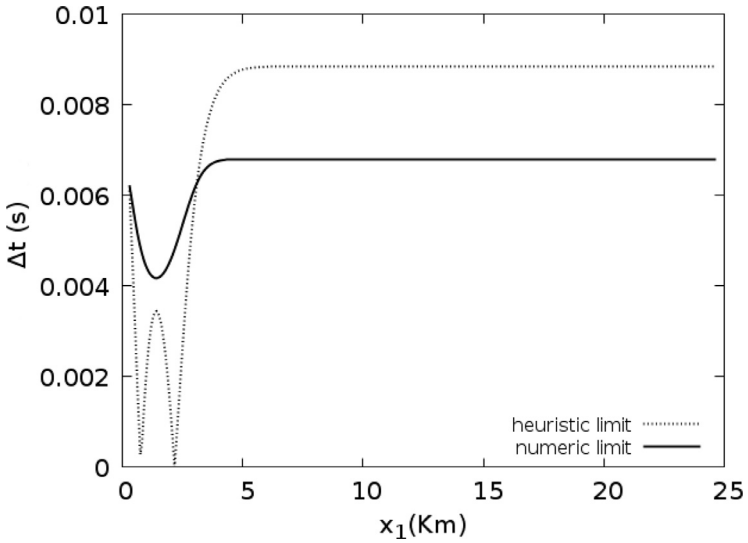

Fig. 4. Stability condition for the Riemannian acoustic wave equation with an upper boundary given by a Gaussian function.The solid line corresponds to the numerical solution of the expression (25). The minimum Δt for the numeric limit is $4.1 \times 10^{-3} s$ and for the heuristic limit is 1.8×10^{-6}.

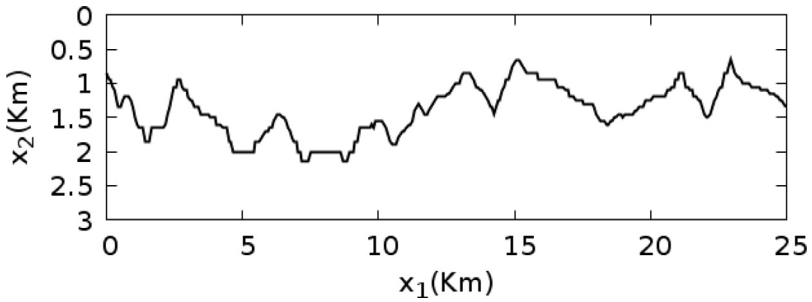

Fig. 5. Boundary of a sub-sampled model of the Canadian Foothills with size 334x200.

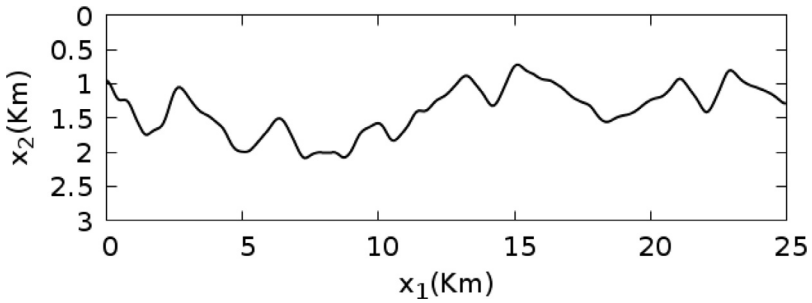

Fig. 6. Smoothed boundary using a moving average, for the sub-sampled model of the Canadian Foothills model.

To derive the dispersion relation, the harmonic plane wave in Eq. (27) is used in Eq. (16), to obtain

$$
\begin{aligned}
2\cos(\omega\Delta t) = 2 + v^2(\Delta t)^2 \Bigg[& \frac{-2g_{11}}{\Delta\xi_1^2} + \frac{2\cos(d\xi_1 p\cos(\theta))g_{11}}{d\xi_1^2} \\
& - \frac{\sin(d\xi_1 p\cos(\theta))\sin(d\xi_2 p\sin(\theta))g_{12}}{d\xi_1 d\xi_2} - \frac{2g_{22}}{d\xi_2} + \frac{2\cos(d\xi_2 p\sin(\theta))g_{22}}{d\xi_2^2} \\
& + i\frac{\sin(d\xi_1 p\cos(\theta))\zeta_1}{d\xi_1} + i\frac{\sin(d\xi_2 p\sin(\theta))\zeta_2}{d\xi_2} \Bigg] = f(\xi_1, \theta, \Delta\xi_1, \Delta\xi_2, p),
\end{aligned}
\tag{28}
$$

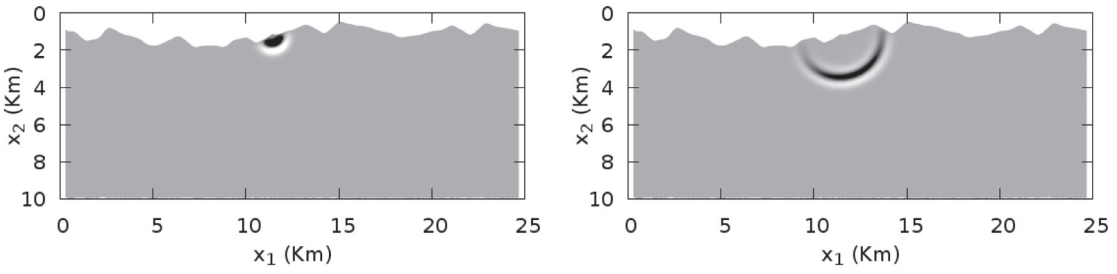

(a) Propagation of the Ricker pulse at 30 ms (b) Propagation of the Ricker pulse at 60 ms

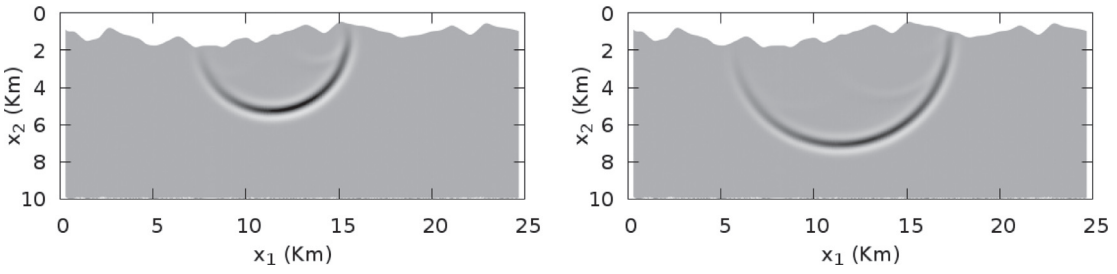

(c) Propagation of the Ricker pulse at 90 ms (d) Propagation of the Ricker pulse at 120 ms

Fig. 7. Snapshots of the propagation of a Ricker pulse in a constant velocity model with a upper boundary corresponding to a sub-sampled version of the Canadian Foothills with size 334x200. The value of Δt used for the propagation was $10^{-3}s$, which is in agreement with the numeric limit shown in Fig. 8 but not with the heuristic limit. The CFL limit for a Cartesian version of this model would be $5.9 \times 10^{-3}s$ which implies that the computational cost is 143% bigger using the Riemannian acoustic wave equation. The mountain boundary was smoothed with a moving average. A secondary wavefront is due to the reflection of the wave in the rugged surface.

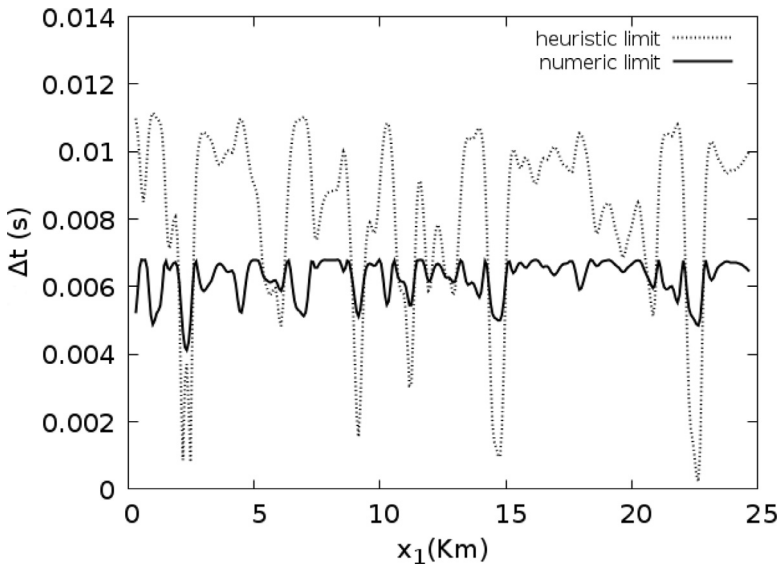

Fig. 8. Stability condition for the Riemannian acoustic wave equation for the sub-sampled Canadian Foothill velocity model. The solid line is the numerical solution of the expression (25). The minimum Δt for the numeric limit is $4 \times 10^{-3}s$ and for the heuristic limit is $2 \times 10^{-4}s$.

where p is the modulus of the wavenumber vector and θ is the argument. Eq. (28) allows to find the relation between the grid points per wavelength $G_1 = \lambda/\Delta\xi_1$, $G_2 = \lambda/\Delta\xi_2$, and the normalized phase velocity $C_p/v = (\omega/k)/v$, since

$$\frac{C_p}{v} = \frac{\omega}{k}\frac{1}{v} = \frac{\omega}{2\pi}\frac{\lambda}{\Delta\xi}\frac{\Delta\xi}{v} = \frac{\omega}{2\pi}G\Delta\xi, \tag{29}$$

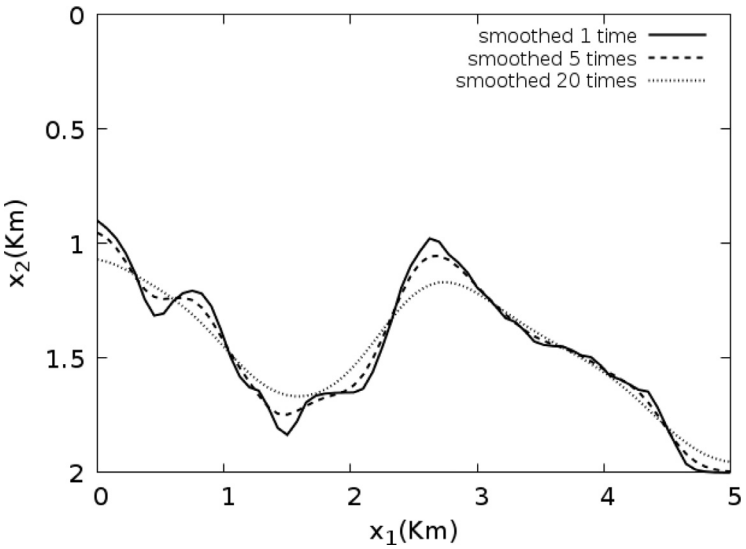

Fig. 9. Smoothed sections for the sub-sampled Canadian Foothills model with different degree of smoothness.

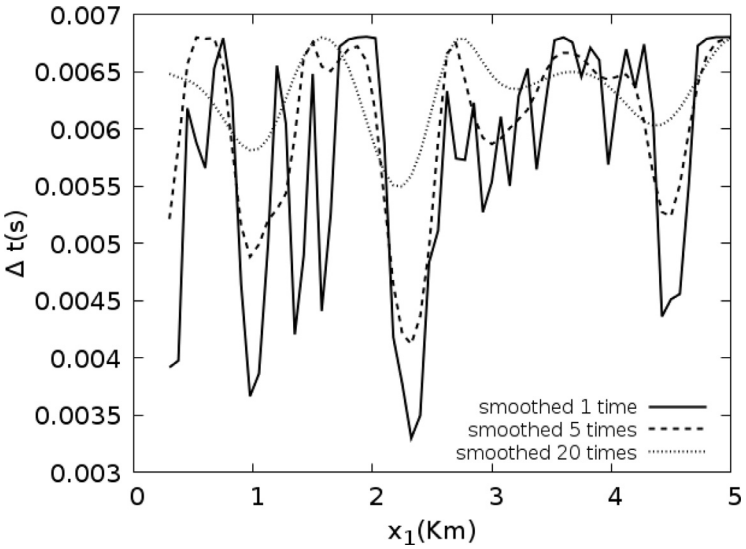

Fig. 10. Maximum Δt allowed for different degrees of smoothness for a section the sub-sampled Canadian Foothills model. The graphs correspond to the boundary shown in Fig. 5, smoothed 1, 5 and 20 times and, the respective limits for Δt are 0.0032 *s*, 0.0041 *s* and 0.0054 *s*.

$$p\Delta\xi = \frac{2\pi}{G}, \tag{30}$$

and

$$\omega\Delta t = \frac{C_p}{v}\frac{2\pi}{G}\frac{v\Delta t}{\Delta\xi} = \frac{C_p}{v}\frac{2\pi c}{G} \tag{31}$$

where $c = v\Delta t/\Delta\xi$ is the Courant-Friedrich-Levy number.

Replacing expression (31) in Eq. (28) we get

$$\frac{C_p}{v} = \frac{G}{4\pi c}\arccos(f(\xi_1, \theta, \Delta\xi, p)), \tag{32}$$

where we take $\Delta\xi_1 = \Delta\xi_2 = \Delta\xi$ for simplicity and f is defined by Eq. (28).

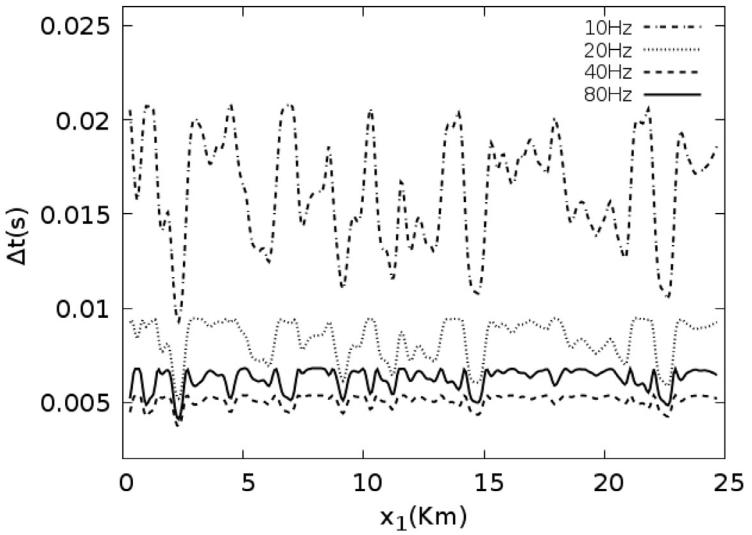

Fig. 11. Maximum Δt allowed for different frequencies. For frequencies bigger than 80*Hz* the curves lie between those of top and the bottom shown.

4. Numerical results

In this section we investigate, the 2D acoustic wave propagation for two topographic coordinates, in the following aspects: (i) stability criteria and, (ii) numerical dispersion. These computational meshes provide informative tests of the generalized 2D acoustic wave equation theory and dummyTXdummy- of the implementation of the 2D FDTD numerical scheme described above.

4.1. Numerical stability

As a first example we solved the acoustic Riemannian wave Eq. (1) for a domain with constant velocity and an upper boundary given by $\psi(x_1) = he^{-a^2x_1^2}$ with $h = 3$ and $a = 0.5$, shown in Fig. 2. Several snapshots for the propagation in that domain are shown in Fig. 3. The stability condition was evaluated numerically using values for Δt from 0.6 s to 0 s and taking the biggest value of Δt that satisfies (25) at each point ξ_1. Since in transformation (9), $\xi_1 = x_1$, we can evaluate the stability condition in terms of x_1 directly. The result are shown in Fig. 4. In Fig. 4 the numeric limit is found by solving numerically the expression (25) and the heuristic limit is the one given by Eq. (15).

As a second example we solved Eq. (1) for a domain with a constant velocity (4 Km/s) and an upper boundary corresponding to the Canadian Foothills velocity model. The size of the model is 1668x1000, nevertheless for our analysis we used a sub-sampled version, taking one sample for each 5 points of the model in both directions. The size of the sub-sampled version used in this work is 334x200. Several snapshots of the propagation of a Ricker pulse in this model are shown in Fig. 7.

Since the calculations of the coefficients ζ_i requires the use of second derivatives, the mountain boundary should be smooth in order to avoid divergences, so we smoothed the original boundary of the sub-sampled model that is shown if Fig. 5 using a simple moving average: the height of each point of the mountain was recalculated as the simple mean of the two nearest neighbors. Fig. 6 shows the result of the application of this moving average after smoothing 5 times. The profile on Fig. 6 is the one used for the propagation in Fig. 7. As shown in Fig. 8, the numeric limit for Δt is bigger than the heuristic limit. Let us define here the *degree of smoothness* of the profile as the number of times it was smoothed with the simple moving average. We evaluated the stability condition (25) for different degrees of smoothness for the profile of Fig. 5 and found that the minimum Δt depends on this degree. The profiles for the several degrees of smoothness we used are shown in Fig. 9 and the respective limits for Δt are shown in Fig. 10.

Additionally we studied the dependence of the condition (25) on the frequency and found that the maximum Δt allowed, strongly depends on the particular values of the frequency used. For the propagation we used a Ricker pulse of central frequency 6*Hz* but it is obviously composed of a wide range of frequencies. Viewing the power spectrum of this pulse we identified a range from 1*Hz* to 80*Hz* approximately, so we evaluated Eq. (25) for different values in this range. The results are shown in Fig. 11.

The results for the stability condition for a section of the Canadian Foothills model at second and fourth order approximations are shown in Fig. 12.

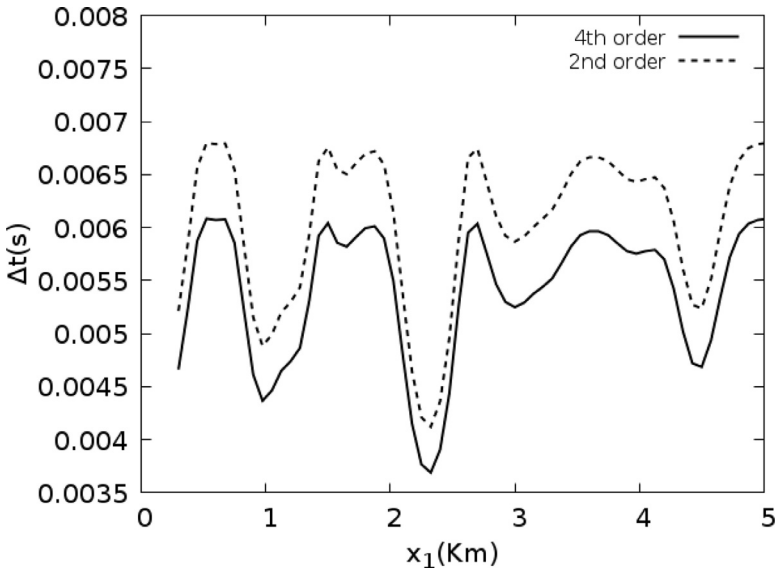

Fig. 12. Comparison of the stability conditions of order 2 and 4 in the spatial derivatives for the Riemannian acoustic wave equation. The maximum Δt allowed for the 2nd order scheme is 0.0041 *s* and for the 4th order is 0.0037 *s*. The frecuency used is 40 Hz.

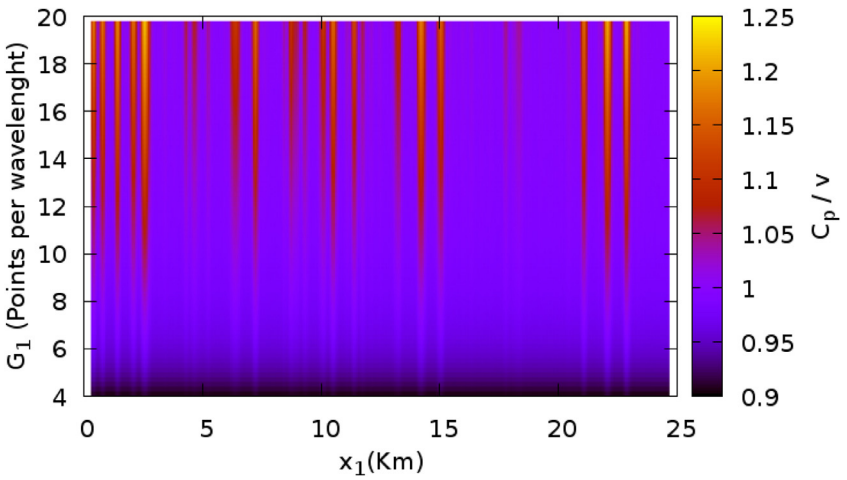

Fig. 13. Dispersion analysis for the sub-sampled Canadian Foothills model with size 334x200. The graph shows that the normalized velocity C_p/v does not get the expected value of 1 for a large number of grid points per wavelength. This plot is for $\theta = 0$.

4.2. Dispersion analysis

Finally, we performed a dispersion analysis using Eq. (32), which allows to observe the variation of the normalized velocity C_p/v as the number of points per wavelength varies. Fig. 13 shows the result when we take the an angle $\theta = 0$ for the wavenumber and Fig. 14 shows the result when the angle is $\pi/2$. For comparisons, we calculated the dispersion for the acoustic wave equation in the Euclidean case and, the result shown in Fig. 15, shows a behavior that is expected: that for a number of points per wavelength large enough the normalized velocity tends to 1. In Fig. 15, after a value of the grid point per wavelength around 14, the normalized velocity remains stabilized. Contrary to the expected result, Fig. 13 shows that no matter the number of point per grid taken, C_p/v is not stabilized, which means that different frequencies have different values of the phase velocity C_p producing wavefronts that are deformed as time runs. This effect is more dramatic for an angle of the wavenumber vector of $\theta = \pi/2$ as shown in Fig. 14.

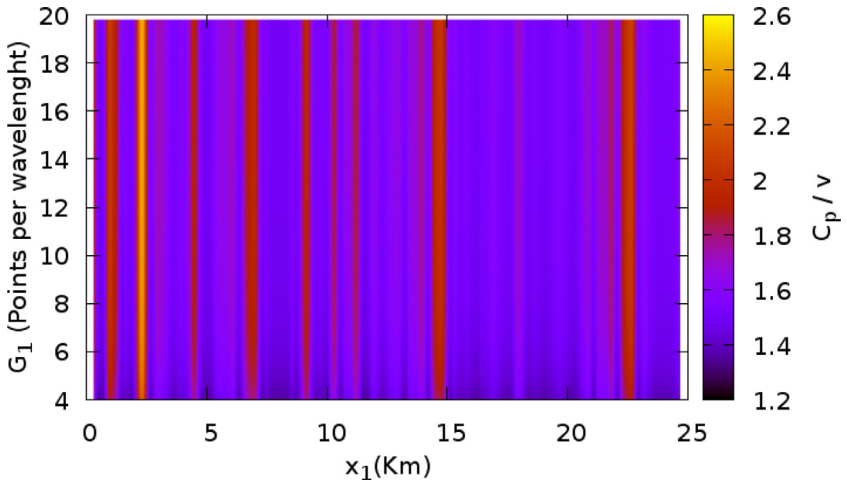

Fig. 14. Dispersion analysis for the sub-sampled Canadian Foothills model of size 334×200. The graph shows that the normalized velocity C_p/v does not get the expected value of 1 for a large number of grid points per wavelength. This plot is for $\theta = \pi/2$.

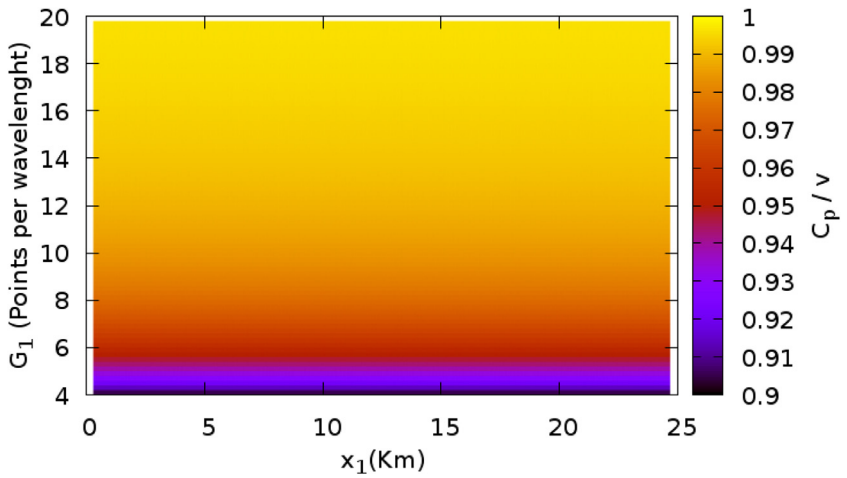

Fig. 15. Dispersion analysis for a constant velocity model with Cartesian metric and flat surface with size 334x200. The graph shows that the normalized velocity C_p/v get the expected value of 1 for a large number of grid points per wavelength.

5. Conclusions

The numerical experiments show that the time step implied by the stability condition strongly depends on the degree of smoothness of the topographic profile so, to obtain time steps suitable for calculations we must represent the topography with curves that may not perfectly match each point of the true profile.

There is a clear difference between the time step given by the heuristic stability condition and the time step given by the limit obtained rigorously.

The limits obtained for the time sampling show that the computational cost of the propagation using a FDTD scheme for the Riemannian 2D acoustic wave equation is bigger than the same simulation with the usual acoustic wave equation (around 143%) bigger for a particular case shown.

Different transformations from the physical domain onto the computational domain, imply different metric tensors and then, different limits for the time step required for stability.

This kind of transformations imply very strong numerical dispersion which suggests that the Riemannian approach to the solution of the acoustic wave equation does not seem to be convenient for RTM or FWI.

The stability and numerical dispersion analysis for other kind of transformation of domains can be achieved using the same general expressions given in this work, just by replacing the corresponding metric tensor.

An analogous analysis can be made for 3D Riemannian wave propagation by defining an appropiate boundary map (coordinate chart $\boldsymbol{\phi}$). We would expect to find similar numerical results for the stability analysis in a 3D scenario, i.e, strong

depence of the numerical stability on the smoothness degree of the topographic profile and a notorious numerical dispersion as in the 2D case.

Acknowledgments

This work is supported by the Colombian Petroleum Company ECOPETROL and COLCIENCIAS, as part of the research project with reference number 0266-2013. The authors want to thank the advices and reviews given by Professor Diego Alberto Gutierrez I., Professor Luis Fernando Duque and Professor Jairo Alberto Villegas I.

References

[1] D. Appelo, A. Peterson, A stable finite difference method for the elastic wave equation on complex geometries with free surfaces., Commun. Compt. Phys 5 (1) (2009) 84–107.
[2] R. Courant, K. Friedrichs, H. Lewy, On the partial difference equations of mathematical physics., Mathematische Annalen 100 (1928) 32–74.
[3] Z. Fu, W. Chen, P. Wen, C. Zhang, Singular boundary method for wave propagation analysis in periodic structures., J. Sound Vibr. 425 (2018) 170–188.
[4] J. Gazdag, Wave equation migration with the phaseshift method., Geophysics 43 (1978) 1342–1351. Special Section - Geothermal
[5] S.H. Gray, K.J. Marfurt, Migration from topography: Improving the near-surface image., Can. J. Expl. Geophys 31 (1/2) (1995) 18–24.
[6] H.W. Guggenheimer, Differential geometry., in: Dover Books on Mathematics, 1977.
[7] S. Hestholm, B. Ruud, A 3-d finite-difference elastic wave modeling including surface topography., Geophysics 63 (1998) 613–622.
[8] M. Karimi, P. Croacker, N. Kessissoglou, Boundary element solution for periodic acoustic problems., J. Sound Vib. 360 (2016) 129–139.
[9] J. Marsden, T. Hughes, Mathematical Foundations of Elasticity., Dover Publications INC, New York, 1983.
[10] J. Robin, D. Salamon, Introduction to Differential Geometry., ETH Zurich, 2013. Lecture notes.
[11] R.P. Fletcher, X. Du, J.F. Paul, Reverse time migration in tilted transversely isotropic (TTI) media., Geophysics 74 (6) (2009) WCA179–WCA187.
[12] P. Sava, S. Fomel, Seismic imaging using riemannian wavefield extrapolation., Geophysics 70 (2005) T45–T56.
[13] J. Seok Lee, E. Deckers, S. Jonckheere, W. Desmet, Y. Young Kim, A direct hybrid finite element-wave based modelling technique for efficient analysis of poroelastic materials in steady-state acoustic problems., Comput. Methods Appl. Mech. Engrg 304 (2016) 55–80.
[14] J. Shragge, Riemannian wavefield extrapolation: Nonorthogonal coordinate systems., Geophysics 73 (2008) T11–T21.
[15] J. Shragge, Solving the 3d acoustic wave equation on generalized structured meshes: A finite-difference time-domain approach., Geophysics 79 (2014) 1–16.
[16] J. Shragge, P. Sava, Wave equation migration from topography., in: Proceedings of the 75th SEG meeting Expanded Abstracts, 2005, pp. 1842–1845.
[17] I. Tarras, L. Giraud, P. Thore, New curvilinear scheme for elastic wave propagation in presence of curved topography., Geophys. Prospect. 59 (2011) 889–906.
[18] Y. Wang, H. Zhou, S. Yuan, et al., A fourth order accuracy summation-by-parts finite difference scheme for acoustic reverse time migration in boundary-conforming grids., J. Appl. Geophys. 136 (2016) 498–512.
[19] W.-J. Wu, L.R. Lines, L. HanXing, Analysis of higher-order, finite-difference schemes in 3-d reverse-time migration., Geophysics 61 (3) (1996) 845–856.
[20] H. Zhao, J. Gao, Z. Chen, Stability and numerical dispersion analysis of finite-difference method for the diffusive-viscous wave equation., Int. J. Numer. Anal. Model. 5 (1/2) (2014) 66–78.